JACS
JOURNAL OF THE AMERICAN CHEMICAL SOCIETY
Article
pubs.acs.org/JACS

Effect of Molecular Stacking on Exciton Diffusion in Crystalline Organic Semiconductors

Rui M. Pinto,[†,‡] Ermelinda M. S. Maçôas,[‡] Ana I. S. Neves,[†] Sebastian Raja,[‡] Carlos Baleizão,[‡] Isabel C. Santos,[§] and Helena Alves*[,†,∥]

[†]INESC MN and IN, Rua Alves Redol 9, 1000-029 Lisboa, Portugal
[‡]CQFM and IN, Instituto Superior Técnico, Universidade de Lisboa, Av. Rovisco Pais, 1049-001 Lisboa, Portugal
[§]C[2]TN, Instituto Superior Técnico, 2695-066 Bobadela, Portugal
[∥]Department of Chemistry, CICECO, University of Aveiro, 3810-193 Aveiro, Portugal

Supporting Information

ABSTRACT: Exciton diffusion is at the heart of most organic optoelectronic devices' operation, and it is currently the most limiting factor to their achieving high efficiency. It is deeply related to molecular organization, as it depends on intermolecular distances and orbital overlap. However, there is no clear guideline for how to improve exciton diffusion with regard to molecular design and structure. Here, we use single-crystal charge-transfer interfaces to probe favorable exciton diffusion. Photoresponse measurements on interfaces between perylenediimides and rubrene show a higher photocurrent yield (+50%) and extended spectral coverage (+100 nm) when there is increased dimensionality of the percolation network and stronger orbital overlap. This is achieved by very short interstack distances in different directional axes, which favors exciton diffusion by a Dexter mechanism. Even if the core of the molecule shows strong deviation from planarity, the similar electrical resistance of the different systems, planar and nonplanar, shows that electronic transport is not compromised. These results highlight the impact of molecular organization in device performance and the necessity of optimizing it to take full advantage of the materials' properties.

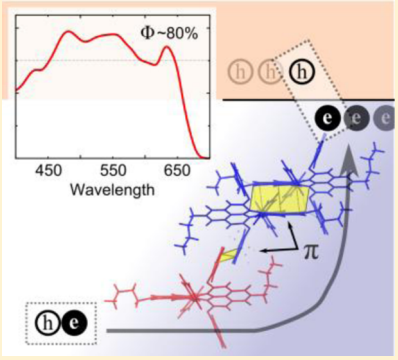

I. INTRODUCTION

The operation of organic photovoltaic and photoconductive devices requires the efficient formation, diffusion, and dissociation of excitons. Exciton formation can be maximized through the use of chemical design to yield an extended spectral range for light absorption by using multilayer semiconductors with different spectral coverages and regulating the thickness and organization of the active layers. Furthermore, the combination of electron-donating and -accepting materials facilitates the dissociation of excitons, which then diffuse to the charge-transfer heterojunction. Yet, exciton diffusion and length[1,2] (L_D) impose severe restrictions on the architecture of charge-transfer heterojunctions due to the short L_D of organic semiconductors. In amorphous and polycrystalline films of organic molecules, like poly(3-hexylthiophene) (P3HT),[3,4] excitons hop via a weak, singlet-limited Förster mechanism, and L_D is usually small (~10 nm) due to nondirectional energy transfer. For optoelectronic devices based on the combination of such small L_D materials, as in polymer/fullerene solar cells,[5,6] the intermixing of donor and acceptor materials in bulk heterojunctions reduces the average distance that an exciton has to diffuse to reach a nearby dissociating interface. However, this approach can also boost electron−hole recombination[7−10] and reduce the available pathways for charge carrier extraction.[11]

Some organic materials, like diindenoperylene,[12,13] show an above average singlet L_D in thin films (60−100 nm), but in single-crystals, L_D may reach micrometer sizes. Indeed, in rubrene, an organic donor material that crystallizes following a herringbone pattern, L_D settles at ~200 nm in epitaxial films[14] but can reach several micrometers in single crystals.[15,16] Moreover, in single crystals, the structural disorder effect is negligible and the highly organized molecular lattices promote orbital overlap, improving charge transport.[17−19] The origin of the micrometer L_D in rubrene is in the long-lived triplet excitons that diffuse through a Dexter mechanism.[15] Acceptor materials like perylenediimides (PDIs), whose optoelectronic properties can be controlled by functionalization at *peri*, *bay*, and *ortho* positions,[20−23] can also yield long-range energy transfer even for singlet excitons.[24] Several strategies have been envisioned to induce longer L_D, such as promotion of singlet fission to increase the yield of long-living triplets.[20] However, there are many constrains to singlet fission, such as unfavorable energetics and demanding interactions between chromophores, which limit the number of organic semiconductors that can efficiently induce singlet fission to a point that is not even considered in the Jablonski diagram.[25] Other strategies to

Received: December 26, 2014
Published: May 20, 2015

DOI: 10.1021/ja512886h
J. Am. Chem. Soc. 2015, 137, 7104−7110

Table 1. Structural Information of Single Crystals of Rubrene and PDIBs as Well as the Interface Plane for Each Crystal Layer

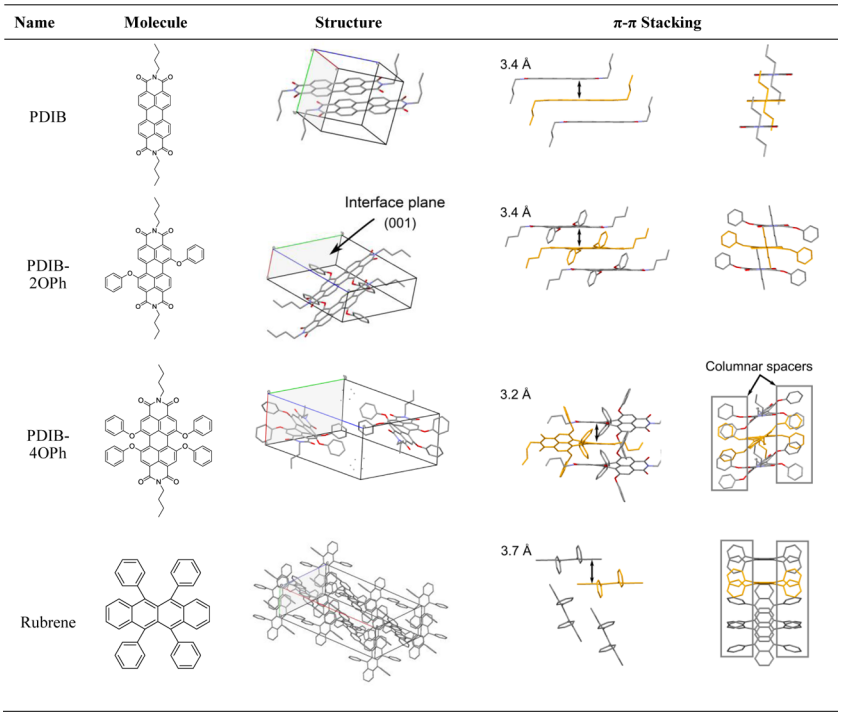

harvest the efficiency of exciton transport, such as a material design guideline, are still unclear.[26] In solution, an intermolecular separation and relative orientation for TIPS-pentacene that induces a triplet formation rate that reaches the diffusion limit has been recently established.[27] Yet, most operating optoelectronic devices are in the solid state, for which there is not an optimal molecular arrangement to follow. For instance, the herringbone structure of rubrene is different from the $\pi-\pi$ slip-stacked structure of *ortho*-benzene-substituted PDI,[20] but both show a significant enhancement of exciton diffusion. Although the exciton diffusion process is still not well-characterized, it is known that intermolecular separation has an exponential impact on the rate of energy transfer.[28] Moreover, at distances lower than ∼8 Å, the dominant energy transfer mechanism is Dexter transfer, even for singlets.

II. EXPERIMENTAL METHODS

II.A. Materials and Crystal Growth. Rubrene (Alfa Aesar, 97%) was used as purchased. PDIB, PDIB-2OPh, and PDIB-4OPh were synthesized according to procedures described in the literature.[29−31] All crystals were grown using the physical vapor transport (PVT) technique[32] under a stream of ultrapure Ar gas. Sublimation temperature for rubrene was around 310 °C, resulting in thin (<1 μm) platelet-like crystals, after a 30−40 min growth period. Sublimation temperature for the different PDIBs was around 375 °C. Thin and elongated PDIB single crystals were obtained after a growth period of several hours. Crystal selection was performed under microscope inspection. Only those crystals with uniform and smooth surfaces were collected and used for lamination.

II.B. X-ray Crystallography. Crystals suitable for X-ray diffraction studies were mounted on a loop with protective oil. X-ray data were collected at 150 K in the ω and φ scans mode on a Bruker APEX II CCD diffractometer using graphite monochromated Mo Kα radiation (0.71073 Å) and operating at 50 kV and 30 mA. Further details can be found in the Supporting Information.

II.C. Interface Fabrication. Devices were fabricated by laminating a crystal on top of thoroughly cleaned glass substrates (piranha solution, DI, acetone, and IPA) and then gently laminating a second crystal on top of the first. Thickness of the crystals was measured by surface profilometry (Dektak 3030ST) after interface assembly. Contacts were formed using carbon paste (PELCO, nr. 16051). Au wire and Ag epoxy (Chemtronics CW2400) were used for wire bonding. Channel dimensions ($W \times L$) were estimated from microphotographs of the interfaces. All fabrication steps were performed under ambient conditions.

II.D. Characterization Measurements. Current−voltage ($I-V$) characteristics of the interfaces were measured in air, under normal ambient conditions, using a Keithley 237 source measure unit. Samples with nonlinear $I-V$'s were discarded, giving a total of 55 working devices for analysis. For this working set, L was in the range 35−695 μm, W was between 5 and 430 μm, and the mean W/L was 0.22. Photocurrent measurements were obtained in a system composed of a 250 W quartz tungsten halogen lamp, a monochromator, and a ThorLabs S121C Si calibrated photodiode. A long-pass filter with a 550 nm cut-on wavelength was used to block eventual second-order reflections above 550 nm. Samples (with contacts) were irradiated at normal incidence, using nonpolarized light, through the (a,b) facet of the PDIB crystals. Irradiation was also performed through rubrene crystals for comparison. Operating light power was in the range 5−10 μW at 500 nm, for a beam spot size of ∼1 mm^2. Under these conditions, photocurrent showed linear behavior with light power and no sample degradation was observed. Absorbance spectra of the interfaces and isolated crystals were measured using a scientific grade spectrometer (QE650000, Ocean Optics), operating in the 200−950 nm range, coupled to a deuterium tungsten halogen light source. Illumination and detection were done in the same geometry as that for the photocurrent measurements and without accounting for reflectivity. The photocurrent yield was calculated as $\Phi = (hc/e\lambda)\cdot[R/(1-10^{-A})]$, where h is Planck's constant, c is the speed of light, e is the electron charge, λ is the excitation wavelength, R is the responsivity, and A is the absorption, normalized for rubrene. For the blends, the absorbance spectra in the 300−2500 nm range were measured using a Shimadzu UV-3101 spectrophotometer with a photomultiplier and PbS detector. Electrochemical data were obtained by cyclic voltammetry in solution (see Supporting Information for further details).

DOI: 10.1021/ja512886h
J. Am. Chem. Soc. 2015, 137, 7104−7110

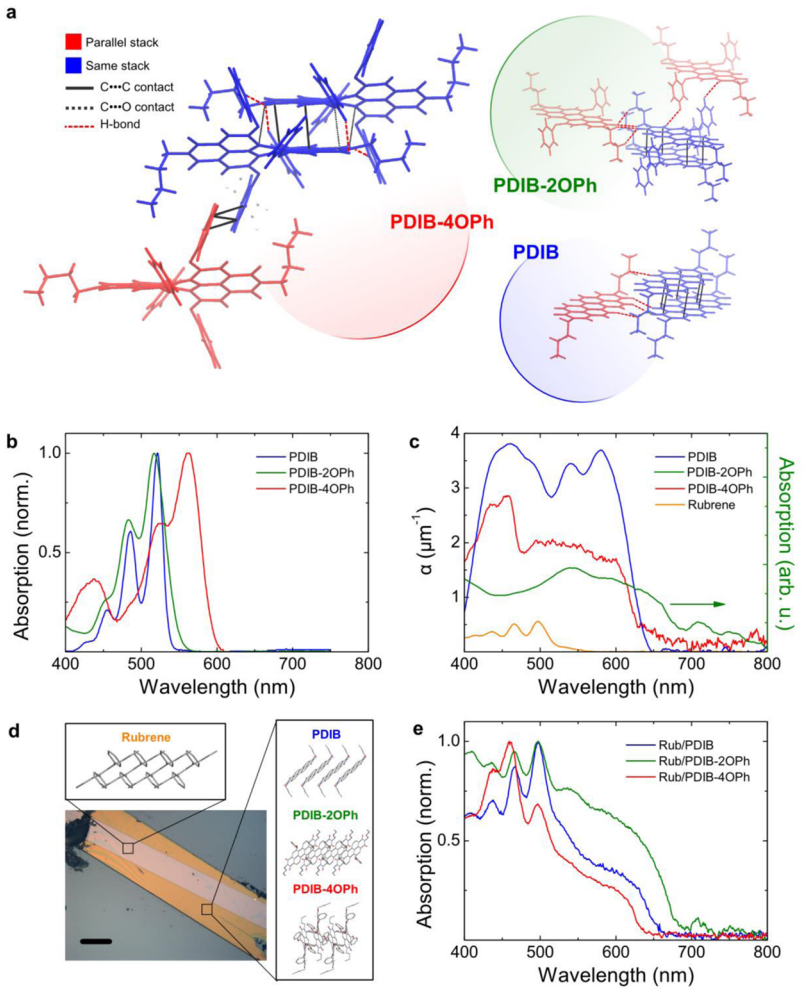

Figure 1. (a) Detail of the chemical structure of PDIB (blue circle), PDIB-2OPh (green circle), and PDIB-4OPh (red circle) showing the intra- and interstack short interactions. The blue molecules represent molecules within the same stack, whereas red molecules represent molecules in a neighboring stack. (b) Normalized absorption spectra of the PDIBs in solution. (c) Absorption coefficient measured in thin (<500 nm) single crystals of the different individual compounds. PDIB-2OPh absorption spectrum is given in arbitrary units because it was not possible to measure an accurate absorption coefficient. (d) Optical microscopy of a rubrene/PDIB single-crystal interface with carbon paste contacting the interface (scale = 100 μm). The boxes show top-view structures of the molecular packing parallel to the interface plane, along the longest axis, for rubrene and the PDIBs. (e) Normalized absorption of the different rubrene/PDIBs interfaces assembled from thin SCs through lamination. The absorption profile of the interfaces almost exactly follows that resulting from the sum of the isolated crystals' profiles.

III. RESULTS AND DISCUSSION

In this work, we present a strategy for molecular organization that enforces exciton diffusion with improved efficiency. This was achieved by using charge-transfer interfaces of single crystals of rubrene and butyl-perylenediimides derivatives (PDIBs) whose structure is varied by chemical design. These crystalline heterojunctions combine high charge separation and quantum yield efficiencies with the high mobility observed in SCs.[33,34] Assembly by the lamination technique ensures the chemical integrity of the interfaces,[33,35] and, in favorable cases, excitons formed at both donor and acceptor materials can be harvested.[36] The interfaces present a photoresponse covering almost all of the visible region (400−650 nm), but the photocurrent yield remains high over the entire spectral range only in one system. By crystal structure analysis, we relate the photoresponse performance to the enhanced energy transfer and increased dimensionality of the percolation network, which depends on short-contact abundance and interaction type.

5,6,11,12-Tetraphenyltetracene (rubrene), *N*,*N*′-butyl-3,4,9,10-perylenediimide (PDIB), and *bay*-area substituted *N*,*N*′-butyl-3,4,9,10-perylenediimide-1,7-phenoxy (PDIB-2OPh) and *N*,*N*′-butyl-3,4,9,10-perylenediimide-1,6,7,12-phenoxy (PDIB-4OPh) were grown as solvent-free single crystals in a physical vapor transport (PVT) furnace. All compounds were purified by at least two recrystallizations. X-ray diffraction (XRD) confirmed the single-crystal nature of PDIBs and the effect of *bay*-area substitution on packing, short contacts, and backbone planarity. The main structural properties obtained from XRD are summarized in Table 1. All compounds are triclinic and centrosymmetric ($P\bar{1}$). Both unsubstituted PDIB and PDIB-2OPh pack cofacially with an interplanar spacing of ∼3.4 Å along the *a*-axis. In PDIB-4OPh, full *bay* substitution leads to a twisted core around the central ring into two planar halves, with a bending angle of 30.8°. In spite of the severe twisting of the core, the two molecular halves are quasi-planar (rms 0.079) and half of the PDI core still presents π-stacking along the *a*-axis, in a zigzag arrangement. Remarkably, their packing distance (3.2 Å) is even smaller than that in the more planar derivatives. In the phenoxy-substituted derivatives, the phenoxy rings act as spacers between adjacent stacking

DOI: 10.1021/ja512886h
J. Am. Chem. Soc. 2015, 137, 7104−7110

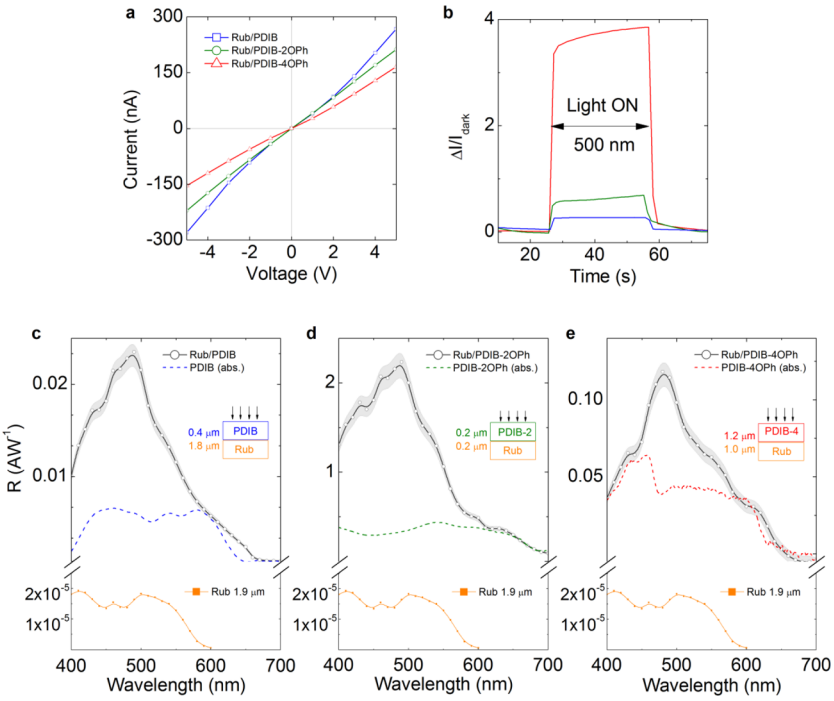

Figure 2. (a) $I-V$ characteristics (dark) of single-crystal interfaces of rubrene and PDIB derivatives. (b) Photocurrent response of the interfaces under 500 nm illumination. The typical responsivity spectra of (c) rubrene/PDIB, (d) rubrene/PDIB-2OPh, and (e) rubrene/PDIB-4OPh, with error bands, are orders of magnitude higher than the responsivity of isolated rubrene SC alone (1.9 μm thick) and show a signal extension of ∼100 nm toward the near-infrared region. The reponsivity of isolated PDIBs is negligible under the same experimental conditions, and the absorption profile of crystalline PDIBs is used for comparison. Panels (c–e) also show the thickness of each single-crystal layer. Illumination is performed through the PDIB layer.

columns. All compounds present intrastack C···C short contacts. However, in PDIB-4OPh, these not only correspond to shorter intermolecular distances (see Tables S2–S4) but also there are C···O, C···H, and O···H short contacts that strongly reinforce the orbital overlap along the stacking direction. Moreover, whereas in PDIB and PDIB-2OPh there are only weak O···H and C···H hydrogen bonds between neighbor columns, in PDI-4OPh there are also C···C contacts with distances of only 2.5–2.9 Å (see Figure 1a), well under the sum of the van der Waals radii. This abundance of strong short contacts along different orientations in PDIB-4OPh increases the dimensionality of the orbital overlap network, although it has a twisted molecular core.

In fact, the concept of optimal π-orbital overlap is more vast than purely maximizing cofacial overlap to improve charge transport.[37]

Figure 1b depicts the absorption profile of PDIB derivatives in solution, showing a bathochromic shift of the absorption onset with increasing *bay* substitution, mainly due to changes in the energy of the lowest unoccupied molecular orbital (LUMO). In fact, PDI derivatives with aryl *bay* substituent groups are, generally, more easily reduced compared to that of unsubstituted PDIs, indicating some delocalization of the LUMO onto the conjugated substituents.[38] This ability of wide color tuning through backbone functionalization is one of the most interesting features of perylene derivatives, which makes PDIs viable alternatives to fullerene derivatives as electron-accepting materials.[39,40] Absorption spectra of isolated PDIB single crystals are shown in Figure 1c and are clearly distinguishable from the absorption profiles measured in solution (Figure 1b). PDIB presents the highest absorption coefficient, $\alpha = 3.8\ \mu m^{-1}$, whereas in PDIB-4OPh, this is lower, $2.9\ \mu m^{-1}$. Due to difficulties in growing large, thin crystals of PDIB-2OPh, we were unable to accurately determine its absorption coefficient. The spectrum presented in Figure 1c relates to a thick PDIB-2OPh crystal with small area; thus, only the spectral profile should be of interest. Sharp vibrational features, as measured in solution, are completely absent in the crystal form as a result of the strong excitonic couplings between the PDIB molecules in the solid state, as observed for Cl-substituted PDIs.[41] In rubrene, the vibrational structure is similar in crystals, in solution, and in thin-film measurements, with no signal over 550 nm and with only small bathocromicity and lower intensity of the 0–0 transition peak at 530 nm.[42]

Optical microscopy of an interface after lamination is shown in Figure 1d, where a long channel rubrene/PDIB ($W \times L = 69 \times 634\ \mu m$) is depicted. Absorption of these interfaces, shown in Figure 1e, almost exactly follows the summed profile of each isolated material, also indicating that no new species are formed. This safeguarding of chemical integrity is unique to donor–acceptor interfaces fabricated via SC lamination[34,35,43] and guarantees the preservation of the morphology and chemical nature at the interface. Further attempts to obtain a rubrene/PDIBs charge-transfer salt by solution blends or by chemical oxidation were also unsuccessful (see Supporting Information), and such a chemical complex is very unlikely to occur under normal conditions.

To evaluate the electrical properties of the interfaces, carbon paste contacts were deposited on the edge of the longest axis of the interface (*b*-axis of rubrene, *a*-axis of the PDIBs), and current–voltage ($I-V$) characteristics were measured at low applied bias ($V_{max} = \pm 5$ V) in a two-terminal configuration. Channel dimensions varied, but the channel length was always higher than 35 μm, minimizing contact resistance. Most

DOI: 10.1021/ja512886h
J. Am. Chem. Soc. 2015, 137, 7104–7110

samples presented a linear $I-V$ curve in a total of 55 samples (Figure 2a), with only a few showing signs of nonlinearity, usually associated with two-probe measurements and bad contacts. Rubrene/PDIB-4OPh samples yield the highest sheet resistance $R_{\square}$ (100−500 MΩ/□), whereas $R_{\square}$ for rubrene/PDI-2OPh was typically around 1−5 MΩ/□. Sheet resistance for rubrene/PDIB interfaces followed a distribution similar to that of rubrene/PDIB-4OPh, with most samples yielding 100−500 MΩ/□. However, for all three PDI derivatives, the interfaces yield a $R_{\square}$ 3 orders of magnitude below the resistivity values of rubrene SC alone, on the order of 1−40 GΩ/□. This same trend is observed in other SC interfaces, such as TTF/TCNQ, TMTSF/TCNQ, and rubrene/TCNQ, where all interfaces had considerably lower resistivity than that of any of its isolated materials.[33,35,43] Such an effect likely comes from the charge transfer between rubrene and PDIB, due to the formation of an induced dipole layer at the interface, and differences in $R_{\square}$ in the three different interfaces can be related with small changes in the LUMO levels of the PDIBs. Indeed, both the absorption spectra (Figure 1a) and the cyclic voltammetry measurements (Table S1) indicate small differences in the LUMO level and gap energy in the PDIBs series. Considering this data, the energy of the PDIBs' LUMO orbital (−3.78 for PDIB-4PhO, −3.32 eV for PDIB, and −3.30 eV for PDIB-2OPh) should favor charge transfer in rubrene/PDIB-4OPh and a lower $R_{\square}$ is expected. However, the twisted structure of PDIB-4OPh probably hinders charge transport, affecting the $R_{\square}$ value of rubrene/PDIB-4OPh.

We then examined the interfaces of rubrene/PDIBs by studying their optoelectronic properties. As presented in Figure 2b, all interfaces show photoconductivity at 500 nm, at an applied bias of 5 V, with samples based on rubrene/PDIB-4OPh yielding the best light-to-current conversion (4 times the current measured in the dark). Figure 2c−e shows the responsivity (R) spectra of the interfaces taken at 5 V applied bias, from 400 to 700 nm, which are compared to the absorption profile of crystalline PDIBs and the responsivity of a bare rubrene crystal (1.9 μm thick). The responsivity is defined as $R = (I_l - I_d)\cdot A_i^{-1}/(P\cdot A_b^{-1})$, in AW^{-1}, where I_l is current under illumination, I_d is current in the dark, P is the light power, A_i is the interfacial area, and A_b is the area of the light beam (~2 mm^2). The absolute maximum responsivity was obtained near 500 nm, with PDIB and PDIB-4OPh yielding lower values (0.01−0.2 AW^{-1}) at this wavelength than those of rubrene/PDIB-2OPh (0.5−2.0 AW^{-1}). In all of them, the responsivity is higher than that measured for bare rubrene SCs of similar thickness, which typically presents a responsivity below 1 mAW^{-1}. Under the same experimental conditions, the PDIBs do not present a measurable photoresponse.

Between 400 and 500 nm, the contribution from rubrene's primary excitons is clearly observed for all three interface types, with rubrene's vibrational features[42] standing out from a broad band. Until 550 nm, both materials absorb; however, the contribution from the PDIBs should be minimal since, typically, PDI derivatives have exciton diffusion lengths (L_D) of only a few tenths of a nanometer, much lower than that of rubrene and the sample thickness. In fact, for PTCDA, the single-crystalline limit for singlet L_D is ca. 25 nm,[44] whereas triplet excitons in rubrene crystals travel at least 2−8 μm without recombining.[15] Only from 550 nm onward can the significant photocurrent generation be independently attributed to the acceptor material (PDIBs), as seen also in PCBM/rubrene.[36] In this region, onsets for photocurrent generation differ slightly in each interface type and follow the absorption profiles of crystalline PDIBs: approximately 640 nm in rubrene/PDIB, 680 nm in rubrene/PDIB-2OPh, and 660 nm in rubrene/PDIB-4OPh. This represents a spectral extension of ~100 nm in the interfaces, as compared to the photoresponse of bare rubrene SC alone, which can be attributed only to the PDIBs.

To further support the hypothesis of acceptor excitons as the origin of photocurrent above 550 nm, we illuminated the samples from both sides and compared their responsivity profiles. We note that the light used was nonpolarized and that the light beam was kept at normal incidence with respect to the plane of the interfaces. Figure 3a presents the results obtained

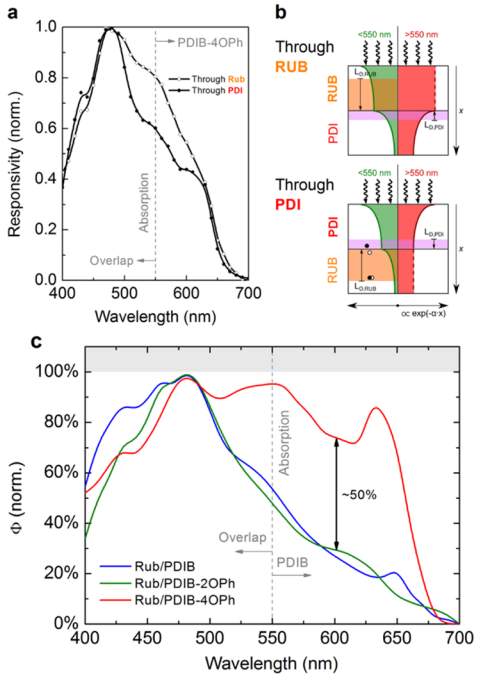

Figure 3. (a) Effect of illumination through rubrene or PDIB-4OPh on the responsivity of an interface. (b) Schematic representation of light attenuation through the sample in relation to exciton diffusion length (L_D) and population, considering illumination through rubrene or PDIBs, at wavelengths where rubrene responds and both donor and acceptor contribute to exciton formation (below 550 nm) and at wavelengths where only the PDIBs contribute (above 550 nm). (c) Normalized photocurrent yield (Φ) of the rubrene/PDIBs interfaces, as measured for illumination through the PDIBs.

for the rubrene/PDIB-4OPh system. When illuminating through rubrene, above 550 nm, an amplified response is observed when compared to illumination through PDIB-4OPh. This observation can be explained on the basis of the proximity of the excitons generated in PDIB-4OPh to the interface, taking in account the differences in exciton diffusion length, the proportion of the population, and the light attenuation through sample depth, illustrated in Figure 3b. Irradiation through rubrene leads to more PDIB-4OPh excitons formed within a few nanometers of the interface, and more photocurrent is generated; in contrast, illuminating through PDIB-4OPh leads to most of the light being absorbed before it reaches a distance $L_{D,\,PDIB}$ from the interface, and fewer PDIB-4OPh excitons will form and diffuse to the interfacial area. A similar trend has also been observed in interfaces using PDIB and PDIB-2OPh, indicating that in these PDIBs excitons do not present long-range diffusion. However, a striking difference among the three

DOI: 10.1021/ja512886h
J. Am. Chem. Soc. 2015, 137, 7104−7110

systems is that the normalized photocurrent yield (Φ) of the rubrene/PDI-4OPh interface presents a high value across all absorption spectra. For the rubrene/PDI-4OPh interface, the yield is higher than 80% from 400 nm until almost 700 nm, whereas in PDIB and PDIB-2OPh, a maximum occurs near 490 nm and sharply decreases with increasing wavelength (Figures 3c and S5).

Analysis of the computed energy levels of rubrene and the PDIBs (see Supporting Information for details) shows that both electron transfer (rubrene to PDIBs) and hole transfer (PDIBs to rubrene) should be energetically feasible ($\Delta G_{CT} < 0$) for all interfaces. Moreover, the computed ionization potentials (IPs) and electron affinities (EA) of PDIB-2OPh and PDIB-4OPh are very similar. This means that hole transfer from these two PDIBs to rubrene should be equally efficient. Since charge-separation (i.e., exciton splitting) efficiency is already optimized at single-crystal CT interfaces,[33] rubrene/PDIB-2OPh and rubrene/PDIB-4OPh interfaces should bear similar, efficient charge-separation processes.

As such, the differences in Φ of the interfaces suggest significant differences in exciton diffusion of PDIBs that is strongly dependent on the orbital overlap between adjacent molecules. In fact, this is the most striking difference among the three systems: the larger intermolecular overlap provided by the molecular organization of PDIB-4OPh. Indeed, the existence of C···C short contacts not only along the same stack but also between parallel stacks as well as the abundance of other short contacts in PDIB-4OPh greatly increases the electronic orbital overlap along different directions (Figure 1a). Such short intermolecular distances impose energy transfer by a Dexter mechanism, which is dominant, even in singlets, for intermolecular distances below 6−8 Å.[45] In this regime, the rate of energy transfer decays exponentially with intermolecular distance.[28] As such, the very short interstack connection in PDI-4OPh of 2.5−2.9 Å, provided by the phenoxy groups, leads to increased exciton diffusion, representing a clear advantage over PDIB and PDIB-2OPh.

IV. CONCLUSIONS

In summary, we have fabricated single-crystal charge-transfer interfaces using rubrene and three perylenediimide derivatives with distinct structural motifs and charge percolation networks. Photoconductivity measurements showed that these high-quality donor−acceptor interfaces yield a wide spectral response in the visible region, extending the response of rubrene alone from 550 to 650 nm with responsivity values between 0.1 and 1.0 AW^{-1} and with an increased magnitude compared to that of bare rubrene. These results clearly show that materials with twisted core structures are not always equated with weak transport characteristics and that strong short contacts across different directions can increase the exciton percolation network to significantly enhance exciton diffusion.

■ ASSOCIATED CONTENT

Supporting Information

Details of the setup and procedure used for the photoresponse measurements; absorption measurements on rubrene/PDIBs blends; cyclic voltammetry of PDIBs in solution; X-ray crystallography, packing details, and short contacts in single-crystals of PDIBs; further details on photocurrent yield calculation; computed energy levels of all materials under study. The Supporting Information is available free of charge on the ACS Publications website at DOI: 10.1021/ja512886h.

■ AUTHOR INFORMATION

Corresponding Author

*alves.helena@ua.pt

Notes

The authors declare no competing financial interest.

■ ACKNOWLEDGMENTS

The authors thank FCT—Fundação para a Ciência e Tecnologia for financial support with grants SFRH/BPD/84820/2012, PTCD/QEQ-SUP/1413/2012, IF/00759/2013, UID/NAN/50024/2013. This work was developed within project Mais Centro-PORC under contract CENTRO-07ST24-FEDER-002032.

■ REFERENCES

(1) Lunt, R. R.; Giebink, N. C.; Belak, A. A.; Benziger, J. B.; Forrest, S. R. *J. Appl. Phys.* **2008**, *105*, 053711.
(2) Akselrod, G. M.; Deotare, P. B.; Thompson, N. J.; Lee, J.; Tisdale, W. A.; Baldo, M. A.; Menon, V. M.; Bulović, V. *Nat. Commun.* **2014**, *5*, 3446.
(3) Shaw, P. E.; Ruseckas, A.; Samuel, I. D. W. *Adv. Mater.* **2008**, *20*, 3516−3520.
(4) Sim, M.; Shin, J.; Shim, C.; Kim, M.; Jo, S. B.; Kim, J.-H.; Cho, K. *J. Phys. Chem. C* **2014**, *118*, 760−766.
(5) Ma, W.; Yang, C.; Gong, X.; Lee, K.; Heeger, A. J. *Adv. Funct. Mater.* **2005**, *15*, 1617−1622.
(6) Liang, Y.; Xu, Z.; Xia, J.; Tsai, S.-T.; Wu, Y.; Li, G.; Ray, C.; Yu, L. *Adv. Mater.* **2010**, *22*, E135−E138.
(7) Keivanidis, P. E.; Ho, P. K.; Friend, R. H.; Greenham, N. C. *Adv. Funct. Mater.* **2010**, *20*, 3895−3903.
(8) Pensack, R. I.; Guo, C.; Vakhshouri, K.; Gomez, E. D.; Asbury, J. C. *J. Phys. Chem. C* **2012**, *116*, 4824−4831.
(9) Li, C.; Wonneberger, H. *Adv. Mater.* **2012**, *24*, 613−636.
(10) Zhan, X.; Facchetti, A.; Barlow, S.; Marks, T. J.; Ratner, M. A.; Wasielewski, M. R.; Marder, S. R. *Adv. Mater.* **2011**, *23*, 268−284.
(11) Keivanidis, P. E.; Howard, I. A.; Friend, R. H. *Adv. Mater.* **2008**, *18*, 3189−3202.
(12) Topczak, A. K.; Roller, T.; Engels, B.; Brütting, W.; Pflaum, J. *Phys. Rev. B* **2014**, *89*, 201203.
(13) Kurrle, D.; Pflaum, J. *Appl. Phys. Lett.* **2008**, *92*, 133306.
(14) Verreet, B.; Heremans, P.; Stesmans, A.; Rand, B. P. *Adv. Mater.* **2013**, *25*, 5504−5507.
(15) Najafov, H.; Lee, B.; Zhou, Q.; Feldman, L. C.; Podzorov, V. *Nat. Mater.* **2010**, *9*, 938−943.
(16) Irkhin, P.; Biaggio, I. *Phys. Rev. Lett.* **2011**, *107*, 017402.
(17) De Boer, R. W. I.; Gershenson, M. E.; Morpurgo, A. F.; Podzorov, V. *Phys. Status Solidi A* **2004**, *201*, 1302−1331.
(18) Menard, E.; Podzorov, V.; Hur, S.-H.; Gaur, A.; Gershenson, M. E.; Rogers, J. A. *Adv. Mater.* **2004**, *16*, 2097−2101.
(19) Molinari, A. S.; Alves, H.; Chen, Z.; Facchetti, A.; Morpurgo, A. F. *J. Am. Chem. Soc.* **2009**, *131*, 2462−2463.
(20) Eaton, S. W.; Shoer, L. E.; Karlen, S. D.; Dyar, S. M.; Margulies, E. A.; Veldkamp, B. S.; Ramanan, C.; Hartzler, D. A.; Savikhin, S.; Marks, T. J.; Wasielewski, M. R. *J. Am. Chem. Soc.* **2013**, *135*, 14701−14712.
(21) Balakrishnan, K.; Datar, A.; Naddo, T.; Huang, J.; Oitker, R.; Yen, M.; Zhao, J.; Zang, L. *J. Am. Chem. Soc.* **2006**, *128*, 7390−7398.
(22) Delgado, M. C. R.; Kim, E. G.; da Silva Filho, D. A.; Brédas, J. L. *J. Am. Chem. Soc.* **2010**, *132*, 3375−3387.
(23) Singh, R.; Giussani, E.; Mróz, M. M.; Di Fonzo, F.; Fazzi, D.; Cabanillas-González, J.; Oldrige, L.; Vaenas, N.; Kontos, A. G.; Falaras, P.; Grimsdale, A. C.; Jacob, J.; Müllen, K.; Keivanidis, P. E. *Org. Electron.* **2014**, *15*, 1347−1361.

DOI: 10.1021/ja512886h
J. Am. Chem. Soc. 2015, 137, 7104−7110

(24) Gregg, B. A.; Spragne, J.; Peterson, M. W. *J. Phys. Chem. B* **1997**, *101*, 5362−5369.
(25) Smith, M. B.; Michl, J. *Chem. Rev.* **2010**, *110*, 6891−6936.
(26) Settels, V.; Schubert, A.; Tafipolski, M.; Liu, W.; Stehr, V.; Topczak, A. K.; Pflaum, J.; Deibel, C.; Fink, R. F.; Engel, V.; Engels, B. *J. Am. Chem. Soc.* **2014**, *136*, 9327−9337.
(27) Walker, B. J.; Andrew, J. M.; Beljonne, D.; Friend, R. H. *Nat. Chem.* **2013**, *5*, 1019−1024.
(28) Menke, S. M.; Holmes, R. J. *Energy Environ. Sci.* **2014**, *7*, 499−512.
(29) Chen, K. Y.; Fang, T.-C.; Chang, M.-J. *Dyes Pigm.* **2012**, *92*, 517−523.
(30) Queste, M.; Cadiou, C.; Pagoaga, B.; Giraudet, L.; Hoffman, N. *New J. Chem.* **2010**, *34*, 2537−2545.
(31) Wurthner, F.; Sautter, A.; Schilling, J. *J. Org. Chem.* **2002**, *67*, 3037−3044.
(32) Laudise, R. A.; Kloc, C.; Simpkins, P. G.; Sigriest, T. *J. Cryst. Growth* **1998**, *187*, 449−454.
(33) Alves, H.; Pinto, R. M.; Maçôas, E. S. *Nat. Commun.* **2013**, *4*, 1842.
(34) Lezama, I. G.; Nakano, M.; Minder, N. A.; Chen, Z.; Di Girolamo, F.; Facchetti, A.; Morpurgo, A. F. *Nat. Mater.* **2012**, *11*, 788−794.
(35) Alves, H.; Molinari, A. S.; Xie, H.; Morpurgo, A. F. *Nat. Mater.* **2008**, *7*, 575−580.
(36) Pinto, R. M.; Maçôas, E. M. S.; Alves, H. *J. Mater. Chem. C* **2014**, *2*, 3639−3644.
(37) Dong, H.; Fu, X.; Liu, J.; Wang, Z.; Hu, W. *Adv. Mater.* **2013**, *25*, 6158−6183.
(38) Huang, C.; Barlow, S.; Marder, S. R. *J. Org. Chem.* **2011**, *71*, 2386−2407.
(39) Guide, M.; Pla, S.; Sharenko, A.; Zalar, P.; Fernandéz-Lázaro, F.; Sastre-Santos, A.; Nguyen, T.-Q. *Phys. Chem. Chem. Phys.* **2013**, *15*, 18894−18899.
(40) Shivanna, R.; Shoaee, S.; Dimitrov, S.; Kandappa, S. K.; Rajaram, S.; Durrant, J. R.; Narayan, K. S. *Energy Environ. Sci.* **2014**, *7*, 435−441.
(41) Graaf, H.; Unold, T.; Mattheus, C.; Schlettwein, D. *J. Phys. D: Appl. Phys.* **2008**, *41*, 105112.
(42) Irkhin, P.; Ryasnyanskiy, A.; Koehler, M.; Biaggo, I. *Phys. Rev. B* **2012**, *86*, 085143.
(43) Nakano, M.; Alves, H.; Molinari, A. S.; Ono, S.; Minder, N.; Morpurgo, A. F. *Appl. Phys. Lett.* **2010**, *96*, 232102.
(44) Lunt, R. R.; Benziger, J. B.; Forrest, S. R. *Adv. Mater.* **2010**, *22*, 1233−1236.
(45) Faure, S.; Stern, C.; Guilard, R.; Harvey, P. D. *J. Am. Chem. Soc.* **2004**, *126*, 1253−1261.

DOI: 10.1021/ja512886h
J. Am. Chem. Soc. 2015, 137, 7104−7110